

LIFT-AND-CRUISE EVTOL BOX-WING CONFIGURATION FOR THE LOW ALTITUDE ECONOMY

Aldo Frediani[1], Emanuele Rizzo[1], Giuseppe Palaia[2], Karim Abu Salem[3] & Marco Martini[1]

[1]SkyBox Engineering, Via G. Caruso 8, Pisa, Italy
[2]Department of Mechanical and Aerospace Engineering, Politecnico di Torino, Torino, Italy
[3]Università degli Studi di Trento, Dipartimento di Ingegneria Civile, Ambientale e Meccanica, Trento, Italy

Abstract

This paper presents the design, development and scaled prototyping of a civil electric vertical take-off and landing aircraft based on the combination of a box-wing lifting architecture and a lift-and-cruise electric propulsion layout. The target operational framework is the low-altitude economy, including civil low-altitude missions such as autonomous logistics, medical transport, inspection, emergency delivery, last-mile cargo, and, in the longer term, urban and extra-urban passenger mobility. The proposed aircraft is conceived as a scalable platform, moving from drone-based applications toward larger advanced air mobility vehicles. Particular attention is devoted to the integration of lateral booms conceived as aerodynamic and structural fairings for the vertical-lift system, allowing the inactive lift rotors to be stowed during cruise. A dynamically reduced scaled model is discussed as a functional demonstrator of the design-to-prototype process, including manufacturing, system integration, preliminary ground verification and low-speed taxi activity.

Keywords: advanced air mobility; box-wing; low-altitude economy; lift-and-cruise; eVTOL

1. Introduction

1.1 Low Altitude Economics

The term low-altitude economy is increasingly used to describe a civil aviation domain centred on dense, short-range operations in near-ground airspace, enabled by the convergence of electric propulsion, increasing automation, digital airspace management, distributed propulsion and new demand for short-duration aerial services. It does not refer only to a market segment, but to an operational ecosystem in which aircraft, ground nodes, communication and surveillance layers, traffic-management services, maintenance procedures and regulatory constraints are coupled from the earliest design stages. In this sense, the low-altitude economy overlaps with urban air mobility and advanced air mobility, but it is broader because it includes unmanned logistics, emergency support, inspection and monitoring missions whose technical requirements are often more immediate than those of routine passenger transport [1–6]. For an aircraft design study, this framing is important because the vehicle cannot be assessed only through isolated hover or cruise metrics. Its architecture affects the feasible mission profile, the ground infrastructure, the safety case, the acoustic footprint and the repeatability of the service.

Representative civil applications include rapid transport of blood products, organs, defibrillators and rescue medications, emergency payload delivery, search-and-rescue support, infrastructure inspection, environmental and territorial monitoring, precision services for distributed assets, last-mile logistics and, in a longer-term perspective, urban, suburban and regional passenger mobility [3, 7–10]. These missions differ from conventional aviation in several respects. Ranges are generally shorter, but flight frequency can be much higher. Turnaround time, recharge or battery-swap logistics, inspection intervals and dispatch reliability can become dominant contributors to operational viability.

Operations take place near populated areas, obstacles and sensitive receptors, where noise, perceived safety, emergency procedures and landing-site compatibility are not secondary constraints. The economic sensitivity of such services is therefore severe: small penalties in mass, drag, cruise efficiency, maintenance complexity or availability may become relevant when the same mission is repeated many times per day.

The vehicle is thus a first-order enabling element of the low-altitude economy, rather than a simple carrier for batteries, sensors or payload. Mission-level efficiency depends on the interaction among hover power, cruise lift-to-drag ratio, installed energy, structural mass, propulsor efficiency and control strategy. Reliability and redundancy must be obtained without excessive mechanical complexity or a disproportionate mass penalty. Maintainability is equally important, since highly distributed operations require aircraft that can be inspected, serviced and returned to operation with limited infrastructure. Infrastructure compatibility also constrains vehicle dimension, footprint, door or payload access, charging interfaces and ground-handling procedures. At the same time, digital airspace concepts for urban and low-altitude operations show that vehicle capability and operating concept are strongly coupled: aircraft with different automation, performance, navigation and contingency characteristics impose different requirements on separation management, route structure and vertiport design [2, 11].

This explains the strong interest in vehicles with vertical take-off and landing capability powered by electricity, the so-called electric vertical take-off and landing aircraft (eVTOL). There are several types of eVTOL aircraft, namely multicopter, tilt-rotor, tilt-wing and lift-and-cruise configurations [11–13]. Multicopters provide direct vertical-lift capability, control simplicity and high redundancy through multiple rotors, and they are attractive for short hover-dominated missions. Their main limitation is due to the absence of the wing, with detrimental effects in forward flight. Tilt-rotor and tilt-wing configurations belong to the category of vectored-thrust aircraft; they exploit wing-borne cruise while using the same propulsive system, or part of it, for vertical and forward flight, and they can improve cruise efficiency but require tilting mechanisms, stronger aero-propulsive coupling and a more demanding transition-control process.

Lift-and-cruise configurations are particularly relevant when cruise represents a substantial fraction of the mission. By separating vertical lift from forward propulsion, the aircraft can retain a fixed wing for cruise while avoiding the full mechanical burden of rotating wings or large propulsors. This is attractive for logistics, medical transport, inspection and regional shuttle missions where the energy spent in horizontal flight cannot be neglected. The separation also allows the cruise propulsors to be sized for a more specific aerodynamic operating point and can simplify the mechanical architecture relative to convertiplanes. However, lift-and-cruise is not free from penalties. Lift propulsors that are inactive during cruise still add mass and, unless carefully integrated, parasitic drag [14]. Their placement influences trim, transition, emergency control, structural loads and the usable payload volume. The transition phase remains a critical part of the flight envelope because lift must be progressively transferred from propulsors to wings without unacceptable attitude excursions, power peaks or loss of controllability [11]. Lift-and-cruise should therefore be considered a promising compromise for cruise-relevant low-altitude missions, not a generally superior architecture. eVTOL aircraft generally exploit distributed electric propulsion, since it offers further degrees of freedom in propulsor placement, redundancy and low-speed control, but it also increases the importance of aero-propulsive interference, acoustic design, wiring, thermal management and structural integration [5, 11].

The endurance problem further indicates that propulsion layout alone cannot solve the aircraft-design challenge. With present electric-storage limitations [15–19], increasing installed battery mass does not produce a proportional increase in useful mission capability, because the additional mass increases the required lift, hover power, structural demand and cruise energy. Improvements in low-altitude aircraft performance must therefore come from a balanced combination of aerodynamic efficiency, compactness, low-speed controllability and airframe-propulsion integration [20]. Compact civil eVTOL aircraft must combine a limited ground footprint with sufficient lifting area, acceptable induced drag, stable low-speed behaviour and a configuration that can host distributed propulsors without excessive interference or mechanical complication [21–25]. For eVTOL aircraft, which fall in the category of unconventional aircraft, the comparison with classical configurations must be mission-

consistent; an arrangement that is not optimal under a conventional transport-aircraft benchmark may become attractive when the design objective includes vertical operation, compact ground infrastructure, high-frequency service and limited installed energy [11, 26].
In this framework, the box-wing configuration can be considered as a candidate lifting architecture for civil low-altitude eVTOL applications. A box-wing is a closed lifting system formed by two staggered horizontal wings connected near the tips by vertical or nearly vertical surfaces. The configuration has a long theoretical background associated with induced-drag reduction in multiplane systems of finite span, and recent studies have reconsidered it because of its potential to combine compact span, favourable lift distribution, structural load paths and payload integration opportunities [27–30]. For low-altitude vehicles, these characteristics may be useful because span and footprint are constrained, while cruise efficiency and low-speed handling remain central to mission economics. The closed lifting system may also provide multiple different locations for propulsor integration and vertical surfaces, and offer structural integrity. These possible advantages depend on wing stagger and vertical gap, interference between horizontal and connecting surfaces, longitudinal and lateral-directional stability, control authority, stall behaviour, aeroelastic effects and the interaction with lift and cruise propulsors [26,28,29,31,32]. A box-wing cannot be treated as an isolated aerodynamic improvement; it must be assessed as an integrated aircraft architecture.
Despite the rapid growth of literature on eVTOL aircraft [33–36], urban air mobility and low-altitude operations, the combined assessment of a box-wing lifting system with a lift-and-cruise propulsion arrangement remains limited. Previous studies on box-wing eVTOL or UAV concepts have mainly considered tilt-wing or broader unconventional arrangements, while the lift-and-cruise literature has generally focused on more conventional wing layouts [11,30]. The gap is wider when the scope is extended from conceptual sizing to configuration definition, propulsion-airframe integration, scaled prototyping and preparation for experimental activity. The present paper addresses this gap by presenting the design rationale, conceptual development, configuration definition and scaled demonstrator of a box-wing lift-and-cruise eVTOL conceived for civil low-altitude operations, from unmanned logistics and utility missions to a possible evolution toward larger advanced-air-mobility vehicles. The paper is organized as follows. Section 2 describes the integrated design workflow, including the design problem, box-wing geometry, hover and cruise power sizing, transition modelling, mass and stability constraints, and the transition from the full-scale concept to scaled prototyping. Section 3 reports the reference configuration, the preliminary design indicators, the scaled prototype implementation, the manufacturing and integration activity, and the first ground-test evidence. Section 4 draws the main conclusions and identifies the subsequent technical developments.

2. Methodology

2.1 Rationale of the integrated design workflow

The methodology adopted in this paper is formulated as an integrated conceptual design workflow for a box-wing lift-and-cruise eVTOL aircraft intended for civil low-altitude operations. The objective is to define a coherent design chain in which the aircraft architecture, mission model, aerodynamic assessment, propulsion sizing, mass estimation and scaled prototyping are treated as connected steps. This distinction is important because low-altitude aircraft are often assessed by isolated figures of merit, such as hover power, number of rotors, maximum endurance or cruise lift-to-drag ratio. These quantities are useful, but they do not determine the feasibility of the aircraft unless they are considered within a mass and energy balance that also includes vertical flight, transition, reserve energy, installed propulsion, stability and ground integration.
The workflow is organised as a design-to-performance chain rather than as a sequence of independent sizing calculations. At the first level, the aircraft is defined by the architectural class, namely a closed box-wing lifting system combined with a separated lift-and-cruise propulsion layout. This choice fixes the main functional allocation of the aircraft, but it does not fix the detailed geometry. At the second level, a mixed set of continuous and discrete variables defines wing span, wing areas, aspect ratios, stagger, vertical separation, lift-rotor diameter, propulsor number and propeller rotational speed; the battery mass is then obtained as the positive residual of the prescribed take-off mass after the remaining mass groups have been evaluated. At the third level, the geometry is con-

verted into aerodynamic and propulsive performance through a build-up estimate of parasite drag, a vortex-lattice estimate of lift distribution and induced drag, hover-rotor sizing, cruise-propeller sizing and electric-machine selection. The last step is the mission-energy post-processing, in which hover, reserve and wing-borne cruise energy are evaluated from the same design state.
This ordering is important because the performance quantities are not independent targets imposed after the configuration has been drawn. Cruise power follows from the drag polar, the selected cruise speed and the propeller efficiency assumed at the operating point; hover power follows from take-off mass, lift-disk area and rotor non-idealities; endurance and range follow from the energy remaining after the vertical-flight, transition and reserve terms have been allocated. The procedure therefore links each performance estimate to the design variables that generate it. A candidate that improves one indicator but violates rotor clearance, tip Mach number, motor power, static margin, wing loading, packaging or energy balance is not retained as a feasible aircraft candidate.
The aerodynamic layer combines component build-up methods and vortex-lattice calculations. The build-up model is used for the parasite contribution in cruise, while the vortex-lattice analysis supports the estimation of lift distribution, neutral point and equivalent induced-drag efficiency of the closed lifting system [37, 38]. In this formulation, the equivalent induced-drag efficiency is not interpreted as the Oswald factor of an isolated conventional cantilever wing. It is an induced-drag parameter associated with the complete box-wing lifting system; values larger than those typical of conventional wings are admissible for closed lifting arrangements and are consistent with the Prandtl-Frediani interpretation of induced-drag reduction in non-planar systems [39, 40].
The configuration is assessed within the assumptions of conceptual design, and the numerical results that follow from the workflow must be understood as preliminary estimates. More detailed analyses, including unsteady transition simulation, high-fidelity aerodynamic interference studies [41], aeroacoustic assessment, structural sizing and failure-case control allocation, are outside the present level of modelling and are identified as subsequent steps. The scaled model is then used as a functional demonstrator of the architecture and of selected integration solutions. It is not interpreted as a direct full-scale performance validation.

2.2 Design problem definition and top-level requirements

The aircraft class considered in the methodology is a lift-and-cruise eVTOL platform with a box-wing lifting system. The vertical-lift function and the forward-thrust function are separated. Dedicated lift rotors provide take-off, landing and low-speed vertical support, whereas dedicated cruise propulsors provide horizontal thrust during wing-borne flight. This functional separation is consistent with missions in which cruise represents a relevant fraction of the total energy demand, and where the mechanical complexity of tilting large lifting surfaces or propulsors is to be avoided. The design problem is therefore defined as the search for an aircraft layout that can provide vertical take-off and landing capability while preserving an efficient fixed-wing cruise segment.
The mission model adopted at conceptual level is composed of a vertical take-off and hover segment, an acceleration and transition segment, a wing-borne cruise segment, a terminal transition segment, and a vertical landing segment. The total available battery energy is written as

$$E_b = e_b m_b, \tag{1}$$

where e_b is the battery specific energy expressed in energy per unit mass and m_b is the installed battery mass. Only a fraction of this energy is available for the mission, because battery management, reserve requirements and operational margins must be retained. The usable energy is therefore written as

$$E_{use} = k_b E_b, \tag{2}$$

where k_b is a usable-energy factor. The cruise energy is obtained after subtracting the energy required by vertical flight, transition and reserve allocation:

$$E_{cr} = k_b e_b m_b - E_{hov} - E_{tr} - E_{res}. \tag{3}$$

The term E_{tr} is kept explicit, rather than being hidden inside an equivalent hover duration, because the transition between rotor-borne and wing-borne flight is one of the critical features of lift-and-cruise

aircraft. When detailed transition data are not available, this term may be evaluated by a conservative conceptual approximation, as described in Section 2.4, or retained as a prescribed design margin.
A useful preliminary range scaling follows from the level-flight energy balance. If m_{TO} is the take-off mass, g is the standard gravity and $(L/D)_{cr}$ is the cruise lift-to-drag ratio, the cruise range can be written as

$$R = \frac{(L/D)_{cr}}{g} \frac{E_{cr}}{m_{TO}}. \tag{4}$$

Substitution of Eq. (3) gives

$$R = \frac{(L/D)_{cr}}{g} \left[k_b e_b \frac{m_b}{m_{TO}} - \frac{E_{hov} + E_{tr} + E_{res}}{m_{TO}} \right]. \tag{5}$$

The same equation can be expressed through the mass balance

$$m_{TO} = m_{str} + m_{sys} + m_{prop} + m_b + m_{pay}, \tag{6}$$

where m_{str} is the airframe structural mass, m_{sys} is the systems and equipment mass, m_{prop} is the propulsion-system mass, m_b is the battery mass and m_{pay} is the payload mass. For a prescribed take-off mass, the battery mass is obtained residually as $m_b = m_{TO} - (m_{str} + m_{sys} + m_{prop} + m_{pay})$ and is required to satisfy $m_b > 0$. This leads to

$$R = \frac{(L/D)_{cr}}{g} k_b e_b \left[1 - \frac{m_{str} + m_{sys} + m_{prop} + m_{pay}}{m_{TO}} - \frac{E_{hov} + E_{tr} + E_{res}}{k_b e_b m_{TO}} \right]. \tag{7}$$

Equation (7) is used only as a conceptual design relation. It shows the coupling among aerodynamic efficiency, battery fraction, structural and system mass, propulsion mass, payload and non-cruise energy. It also clarifies that increasing the battery mass alone is not sufficient to increase useful range if the corresponding mass penalty reduces the remaining mass available for payload, structure and propulsion.
These relations define the analytical backbone of the sizing and performance problem. They also provide the link between the design variables and the mission indicators used to compare feasible candidates. When the design search is oriented toward endurance or range, the ranking quantity can be expressed through the wing-borne energy available after the prescribed non-cruise allocations. With the cruise power evaluated at the selected cruise condition, this objective can be written as

$$t_{cr} = \frac{E_{cr}}{P_{el,C}}, \qquad R = V_{cr} t_{cr}, \tag{8}$$

where $P_{el,C}$ is the electric power required in cruise and V_{cr} is the sizing cruise speed. Equation (8) is a post-processing relation, not an independent performance assumption. The value of $P_{el,C}$ depends on the drag polar, propeller efficiency, motor-drive efficiency and cruise speed generated by the candidate design.
The continuous design vector $\mathbf{x}$ includes, depending on the design iteration, the wing span, front and rear wing areas or aspect ratios, taper ratios, sweep angles, longitudinal stagger, vertical separation, root-chord positions, hover-rotor diameter, propeller rotational speeds and cruise-propeller sizing parameters. In the present implementation, battery mass is not an independent search variable; it is obtained from the mass balance and constrained to remain positive. The discrete design vector $\mathbf{z}$ includes the number of lift rotors, the number of cruise propulsors, motor selections from the preliminary electric-machine database and other architecture-level integer choices, such as the admissible propeller/blade arrangement. The conceptual design problem can therefore be written in the generic mixed discrete-continuous form

$$\begin{aligned} \max_{\mathbf{x},\mathbf{z}} \quad & J(\mathbf{x},\mathbf{z}) \\ \text{subject to} \quad & \mathbf{c}(\mathbf{x},\mathbf{z}) \le \mathbf{0}, \\ & \mathbf{r}(\mathbf{x},\mathbf{z}) = \mathbf{0}, \\ & \mathbf{x}_{min} \le \mathbf{x} \le \mathbf{x}_{max}, \qquad \mathbf{z} \in \mathscr{Z}, \end{aligned} \tag{9}$$

where J may be the achievable range, endurance, payload-range product or a mission-specific energy margin. For an endurance- or range-driven search, J is evaluated after the non-cruise energy terms have been allocated and after the cruise power has been computed from the same aerodynamic and propulsive state. The inequality constraints $\mathbf{c}$ collect hover thrust and power margins, disk loading, tip Mach number, rotor-clearance constraints, cruise thrust and power requirements, battery usable-energy and reserve requirements, static-stability bounds, trim capability and motor/propeller database limits. The equality constraints $\mathbf{r}$ include the aircraft mass-balance consistency condition, the prescribed top-level requirements and, when imposed, the alignment between the centre of gravity and the centre of the vertical-lift thrust system in the nominal hover condition.

When the cruise speed is prescribed by the top-level aircraft requirements, $C_{L,cr}$ is not treated as an independent geometric design variable. It is computed from the current weight, reference area, air density and cruise speed, and is retained in Table 1 only as an aerodynamic sizing/check output constrained to an admissible range. In the alternative sizing mode used by Eq. (19), the same relation can be inverted to infer V_{cr} from a target $C_{L,cr}$.

The design-search structure associated with Eq. (9) is reported in Tables 1 and 2. The formulation is separated into two parts in order to avoid mixing design degrees of freedom and feasibility checks. Table 1 reports each variable or selected discrete quantity on a separate row, together with the search interval or admissible set available in the present preliminary sizing environment. Table 2 reports the objective function and the independent constraints used to accept, reject or rank a candidate design. These limits define the conceptual search domain of the present application. They should not be interpreted as certification requirements or as final installation margins.

Table 1 – Individual design variables and boundaries used in the preliminary mixed discrete-continuous sizing search. The table defines the methodological search space and does not anticipate the numerical design states reported in the results section.

Design block	Individual design variable or selected quantity	Symbol	Boundary or admissible set
Mission and mass	Take-off mass state	m_{TO}	Numerical search state with upper value 3600 kg
Mission and mass	Payload mass	m_{pay}	450–500 kg
Mission and mass	Battery mass allocation	m_b	Residual from the mass balance, $m_b = m_{TO} - (m_{str} + m_{sys} + m_{prop} + m_{pay}) > 0$
Box-wing geometry	Fuselage diameter used for integration	D_{fus}	Fixed equivalent-cylinder diameter defined so that the cylinder wetted area equals the fuselage wetted area obtained from CAD
Box-wing geometry	Span	b	8–14 m
Box-wing geometry	Longitudinal wing stagger	Δx	0.2–14 m
Box-wing geometry	Front-wing aspect ratio	AR_1	8–12
Box-wing geometry	Front-wing taper ratio	λ_1	0.3–1.0
Box-wing geometry	Rear-wing aspect ratio	AR_2	8–12
Box-wing geometry	Rear-wing taper ratio	λ_2	0.3–1.0
Box-wing geometry	Front-wing sweep angle	Λ_1	$-30°$–$20°$
Box-wing geometry	Rear-wing sweep angle	Λ_2	$-30°$–$20°$
Hover propulsive system	Number of lift rotors per half span	$N_H/2$	2–4
Hover propulsive system	Hover motor selection	ID_H	Discrete motor ID 1–229 in the preliminary database
Hover propulsive system	Hover gearbox ratio	N_{prop}/N_{mot}	0.1–10
Hover propulsive system	Hover rotor speed	Ω_H	1000–15000 rpm
Hover propulsive system	Hover rotor diameter	D_H	40–200 in
Hover propulsive system	Rotor blade chord-to-radius ratio	c/R	0.15–0.30
Cruise propulsive system	Cruise motor selection	ID_C	Discrete motor ID 1–229 in the preliminary database
Cruise propulsive system	Cruise propeller speed	Ω_C	1000–15000 rpm
Cruise propulsive system	Cruise propeller pitch-to-diameter ratio	P/D	0.4–1.2
Aerodynamic sizing/check output	Cruise lift coefficient at prescribed TLAR cruise speed	$C_{L,cr}$	Computed from W, S, ρ and V_{cr}; admissible target range 0.2–0.6

Table 2 – Objective function and independent constraints used in the preliminary sizing loop. The values are imposed in the design-search formulation and are therefore methodological inputs, not results of the configurations discussed later. The stated bounds and definitions correspond to the adopted preliminary sizing implementation.

Class	Qualitative meaning	Mathematical or computational statement	Imposed value or bound
Objective	Wing-borne endurance after vertical-flight, transition and reserve allocation	$J = t_{cr} = E_{cr}/P_{el,C}$, with $R = V_{cr}t_{cr}$	Maximize among feasible candidates
Energy balance	Usable cruise energy after non-cruise allocation	$E_{cr} = E_{use} - E_{hov} - E_{tr} - E_{res}$ in the general formulation	Positive residual cruise energy, $E_{cr} > 0$; no prescribed upper bound
Hover installation	Lift-rotor disks compatible with the effective boom length	$D_H N_{side} \leq L_{eff}$	Candidate-dependent L_{eff}
Hover installation	Rotor radius compatible with semi-span clearance	$D_H/2 \leq b/2$	Candidate-dependent semi-span
Packaging	Rotor, door and boom non-overlap proxy	Clearance proxy $\geq R_H$	Exact geometric definition
Fuselage integration	Fuselage length within the adopted installation envelope	$L_{fus} \leq L_{fus,max}$	$L_{fus,max} = 14$ m
Longitudinal stability	Positive static-margin proxy	$(x_{NP} - x_{CG})/\bar{c}_{ref} \geq 0$	Lower bound 0
Trim/stability proxy	Center of pressure/CG distance limited within the conceptual envelope	$(x_{CP} - x_{CG})/\bar{c} \leq 0.5$	Upper bound 0.5
Aerodynamic envelope	Maximum lift coefficient used for stall-speed check	$C_{L,max}$ used in V_{st} estimate	$C_{L,max} = 1.2$; preliminary conservative value for a 14%-thick airfoil with a simple plain flap and no complex high-lift system
Cruise force balance	Cruise thrust-drag residual at the sizing point	$\lvert T_C - D \rvert \leq \varepsilon_T$	$\varepsilon_T = 0.05$; residual normalization
Hover thrust margin	Vertical-lift thrust greater than take-off weight	$T_H/W \geq 1$	Lower bound 1
Hover tip speed	Compressibility/acoustic bound on lift rotors	$M_{tip,H} \leq 0.60$	Upper bound 0.60
Cruise tip speed	Compressibility/acoustic bound on cruise propellers	$M_{tip,C} \leq 0.75$	Upper bound 0.75
Hover motor torque	Hover motor torque within available database value	$Q_H \leq Q_{H,lim}$	$Q_{H,lim} = 500$ Nm in the preliminary database
Hover motor power	Hover shaft power within imposed power margin	$P_H \leq 0.70 P_{H,rated}$	70% of database-rated power
Cruise motor power	Cruise shaft power within imposed power margin	$P_C \leq 0.70 P_{C,rated}$	70% of database-rated power
Cruise static thrust	Static cruise-thrust proxy above minimum installation threshold	$T_{0,C}/W \geq 0.25$	Lower bound 0.25; normalization

The separation between design variables and constraints is methodologically important. The variables in Table 1 define the search space, whereas the constraints in Table 2 define the feasibility filter applied before endurance or range is evaluated. The rotor diameter, for example, is beneficial for reducing disk loading and hover induced power, but it is admissible only if the lateral boom length, blade-stowage condition, semi-span clearance and door geometry remain compatible. Similarly, the cruise propeller is not selected from thrust alone: propeller speed, tip Mach number, motor-power margin and the cruise drag generated by the same aerodynamic state must remain consistent. Battery mass and take-off mass are also coupled: after all other mass groups have been evaluated, m_b is obtained as the positive residual of the prescribed m_{TO}; the resulting stored energy then modifies hover power, wing loading and the mass state from which cruise performance is computed.
Because the problem contains both continuous and discrete variables and relies on preliminary models, the objective is not to claim a unique global optimum. The adopted procedure is instead a disciplined engineering search that rejects infeasible layouts, ranks feasible candidates according to the selected endurance/range objective and keeps each retained configuration traceable to explicit aerodynamic, propulsive, geometric, stability, packaging and mass-energy constraints.

2.3 Aircraft geometry and box-wing architectural variables

The aircraft lifting system is described by two main horizontal wings connected near the tips by vertical or nearly vertical surfaces, forming a closed lifting arrangement in front view. The geometry is parameterised using the span b, the front and rear wing reference areas S_1 and S_2, the corresponding aspect ratios AR_1 and AR_2, taper ratios, longitudinal stagger, vertical separation, sweep angles and relative root-chord positions. For each lifting surface, the basic relation between span, reference area and aspect ratio is

$$AR_i = \frac{b^2}{S_i}, \qquad i = 1,2. \tag{10}$$

The total reference area is

$$S = S_1 + S_2, \tag{11}$$

with the associated wing loading W/S. The distribution of area between front and rear wings is not treated as a purely geometrical choice. It affects lift sharing, induced drag, static margin, trim, structural load paths and the placement of the vertical-lift rotors. Consequently, the geometry is generated in a way that preserves compatibility between aerodynamic performance and the mechanical integration of the lift-and-cruise propulsion system.
The vertical-lift propulsors are located in lateral booms connecting the front and rear lifting elements. This solution is intended to reduce the exposure of inactive vertical-lift propulsors during cruise and to preserve a compact lifting system. At conceptual level, the geometry must satisfy minimum clearance constraints between rotor disks, wing surfaces, booms and movable doors. If D_H is the hover-rotor diameter and $R_H = D_H/2$ its radius, the rotor centre must be placed so that

$$R_H + \Delta_{clr} \leq d_{min}, \tag{12}$$

where d_{min} is the minimum distance from the rotor centre to any interfering airframe boundary and Δ_{clr} is a prescribed clearance allowance.
The aerodynamic assessment of the box-wing system is performed in two steps. A preliminary parasite-drag estimate is obtained through a component build-up method, including the main lifting surfaces, fuselage, booms and exposed installation contributions where available [37, 42]. The induced-drag trend, lift distribution and longitudinal aerodynamic characteristics are then assessed using vortex-lattice analysis. The vortex-lattice model is appropriate for the linear, attached-flow part of the cruise and low-angle-of-attack envelope, and it is used accordingly. It is not used to validate stall behaviour, separated flow, propeller-wing interaction, door-open aerodynamics or transition aerodynamics. These effects require higher-fidelity aerodynamic analyses or dedicated tests.
The component build-up is applied to the cruise, door-closed configuration. The wetted and reference areas of the fuselage, lifting surfaces, vertical tip-wings, booms and exposed installation items are treated as separate contributions, so that the drag penalty of the propulsion-airframe integration remains visible at sizing level. This representation is consistent with conceptual design, because it

preserves the dependency of the cruise power on geometry and installation choices without introducing unsupported high-fidelity corrections. The door-open state is not used to infer the cruise polar; it belongs to the low-speed and transition envelope and requires a dedicated interference analysis.
The vortex-lattice model is used as the lifting-surface layer of the same aerodynamic chain. The front wing, rear wing and vertical tip-wings are represented as lifting panels in the linear attached-flow regime. The model provides lift sharing between the two horizontal wings, the induced-drag trend, the neutral-point estimate and the equivalent induced-drag parameter used in the parabolic polar. Its role is therefore to connect the box-wing geometry to the cruise polar and to the stability quantities used in the sizing loop. Viscous drag, airfoil stall, separated flow at the junctions, rotor slipstream effects and the aerodynamic consequences of open boom doors are not inferred from the vortex-lattice solution.
When the induced-drag contribution is recast into an equivalent parabolic-polar form, the efficiency factor must be interpreted as an equivalent parameter of the closed lifting system, not as the Oswald factor of a conventional cantilever wing. Values larger than those usually expected for conventional aircraft may arise in this formulation because the box-wing arrangement modifies the finite-span lifting system and its induced-drag distribution, consistently with the Prandtl closed-wing rationale and with vortex-lattice assessments of box-wing configurations [27, 28].

2.4 Hover, cruise and transition power sizing

The notation used in the propulsion sizing distinguishes consistently between mass and weight. The take-off mass is denoted by m_{TO}, while the corresponding weight is

$$W = m_{TO} g. \tag{13}$$

In hover, the vertical equilibrium of a configuration with N_H identical lift rotors requires

$$N_H T_H = W, \tag{14}$$

where T_H is the thrust produced by each hover rotor in the nominal symmetric condition. The hover-rotor sizing is based on actuator-disk and propeller relations appropriate to preliminary V/STOL analysis [43]. The total disk area is

$$A_H = N_H \frac{\pi D_H^2}{4}. \tag{15}$$

The ideal induced power in hover can be written as

$$P_{i,H} = \frac{W^{3/2}}{\sqrt{2\rho A_H}}, \tag{16}$$

where ρ is the air density. In the actual sizing, this value is corrected by a figure of merit or an equivalent efficiency factor, and by profile and installation losses. The electric power required for hover is therefore expressed as

$$P_{el,H} = \frac{\kappa_H P_{i,H}}{\eta_{m,H}}, \tag{17}$$

where κ_H accounts for non-ideal rotor and installation effects and $\eta_{m,H}$ is the electrical-to-shaft efficiency of the hover motor and drive system. The hover energy is then obtained from the prescribed hover duration, including take-off, landing and low-speed vertical manoeuvring margins,

$$E_{hov} = P_{el,H} t_{hov}. \tag{18}$$

The motor selection is constrained by shaft power, torque, rotational speed, tip Mach number, rotor diameter and thrust margin. The tip Mach number is limited to reduce compressibility and acoustic penalties, while the disk loading is kept as low as compatible with aircraft footprint and integration constraints.
During cruise, the aircraft is treated as a fixed-wing vehicle. The cruise speed corresponding to a prescribed lift coefficient $C_{L,cr}$ is

$$V_{cr} = \sqrt{\frac{2W}{\rho S C_{L,cr}}}. \tag{19}$$

The cruise drag is evaluated through a parabolic polar,

$$D_{cr} = \frac{1}{2}\rho V_{cr}^2 S\left(C_{D0} + KC_{L,cr}^2\right), \tag{20}$$

where C_{D0} is estimated by the build-up method and $KC_{L,cr}^2$ is the induced contribution assessed by means of the vortex-lattice solver. The cruise propulsive system is not sized from a static-thrust requirement equal to aircraft weight. It is sized from the thrust and power required in forward flight, with additional margins for climb, acceleration, transition and thermal operation. The minimum cruise thrust requirement is

$$T_C \geq D_{cr}, \tag{21}$$

while the electric power required in level cruise is

$$P_{el,C} = \frac{D_{cr} V_{cr}}{\eta_{p,C}\eta_{m,C}}, \tag{22}$$

where $\eta_{p,C}$ and $\eta_{m,C}$ are the cruise propeller and motor-drive efficiencies. The final motor and propeller selection must also satisfy rotational speed, torque, diameter, tip-speed and available-power limits.

The propeller model is kept at sizing fidelity and is expressed through the standard non-dimensional quantities

$$J = \frac{V}{nD}, \qquad C_T = \frac{T}{\rho n^2 D^4}, \qquad C_P = \frac{P_s}{\rho n^3 D^5}, \tag{23}$$

where n is the rotational speed in revolutions per second and D is the propeller diameter. In forward flight, the propulsive efficiency is written as

$$\eta_p = \frac{JC_T}{C_P}. \tag{24}$$

The hover-rotor calculation corresponds to the low-advance-ratio limit and is anchored by the actuator-disk estimate of Eq. (16), corrected through the non-ideal factors introduced above. The cruise propeller is instead evaluated at the wing-borne operating point, where diameter, rotational speed, pitch-to-diameter ratio, tip Mach number and required shaft power are constrained simultaneously. The adopted formulation is adequate for ranking candidate configurations and estimating power levels, but it is not a replacement for blade-element analysis, propeller-map generation or aeroacoustic assessment.

The electric-machine integration is treated consistently with the preliminary nature of the design loop. For each candidate propulsive installation, the rotor or propeller calculation provides the required shaft power and rotational speed. The corresponding shaft torque is

$$Q = \frac{P_s}{\Omega}, \tag{25}$$

where P_s is the shaft power and Ω is the angular speed. The motor selection is then checked against the available entries of the preliminary database by using power, speed, torque when the torque information is available, and a sizing margin on the available motor power,

$$P_s \leq \sigma_P P_{rated}, \tag{26}$$

where σ_P is the adopted power-margin factor. The same logic is applied to the hover motors and to the cruise motors, although the two installations have different operating points: the hover group is dominated by static thrust, disk loading and low-speed induced power, while the cruise group is dominated by propeller efficiency, shaft power, rotational speed and tip Mach number in wing-borne flight.

At this level of modelling, the cruise propulsion group is therefore assessed through the quantities that are directly supported by the preliminary sizing chain: required shaft power, propeller diameter, rotational speed, available motor-power margin and mission-energy consequence. Detailed motor-drive

matching, including the final torque margin, inverter limits, thermal derating and possible transmission architecture, belongs to the propulsion-installation refinement. The performance table consequently reports cruise power and energy indicators, but it does not present unsupported conclusions on the definitive torque margin of the motor-drive installation.

The electric-machine selection is supported by a preliminary motor database assembled from available manufacturer data and published specifications. Each entry contains, when available, the manufacturer, model, mass, power rating used by the sizing loop, torque, voltage class and maximum rotational speed. The database is used in two different ways. First, it provides discrete motor candidates for the hover and cruise propulsive groups. Second, it defines a power-to-mass trend used to avoid unrealistically optimistic extrapolations when a candidate lies outside the directly tabulated range. Entries without torque data are retained for power-mass trend assessment, but they are not used to demonstrate torque feasibility.

The high-power entries relevant to the present sizing were checked against publicly available specifications. For example, the EMRAX 268 data are consistent with a motor mass of about 21.4–22.3 kg, a peak power of 210 kW, continuous power up to 117 kW, peak torque of 500 Nm and continuous torque up to 250 Nm. The current EMRAX 348 specification reports a mass of about 43.1–43.9 kg, peak power of 340 kW and continuous power up to 140 kW, with torque ratings depending on the operating definition. The Siemens SP260D public factsheet reports a 260 kW continuous aircraft motor, 2500 rpm maximum continuous speed, approximately 1000 Nm continuous torque and 50 kg system weight including the propeller bearing [44–46]. These comparisons confirm the order of magnitude of the database, but they also show why the database cannot be interpreted as a final motor-drive qualification: continuous, peak and short-duration ratings depend on cooling, controller capability, drive cycle and installation conditions.

Figure 1 reports the power-mass distribution used for this preliminary assessment. The solid curve is a power-law fit of the available entries above 5 kW, while the dashed portion represents only the extrapolated continuation of the same trend beyond the directly populated high-power range. This extrapolated trend is used as a conservative design aid and not as evidence that a specific commercial motor exists at the extrapolated point.

In log-log form, the fitted relation is

$$P_{db} = 5.50\, m_{mot}^{0.875}, \tag{27}$$

where P_{db} is expressed in kW and m_{mot} in kg. The coefficient of determination of the log-log fit for database entries above 5 kW is $R^2 = 0.906$.

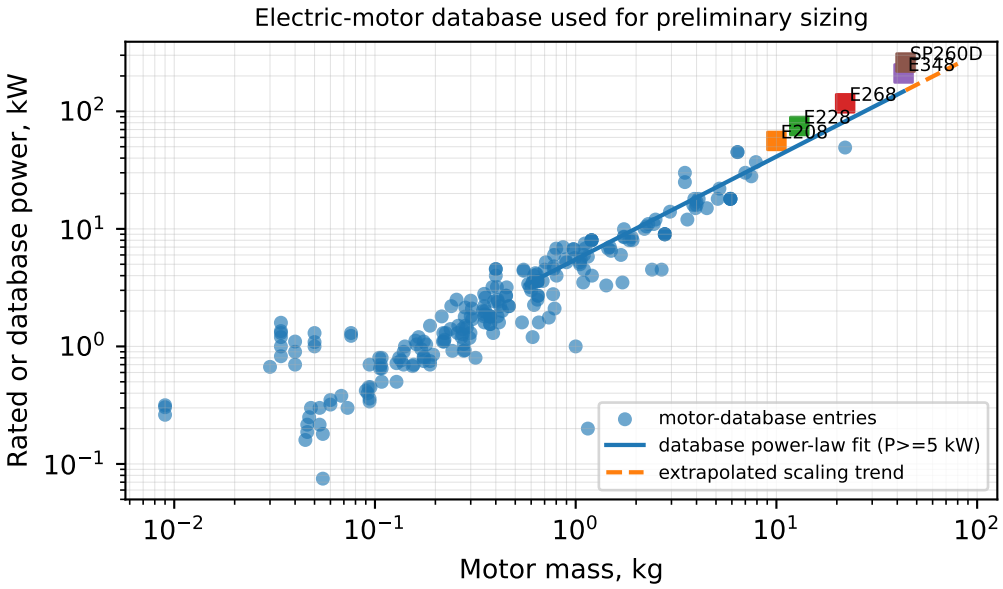


Figure 1 – Electric-motor power-mass chart used for preliminary propulsion sizing.

A simplified transition model is introduced only as a conceptual sizing check. It is not a substitute for a six-degree-of-freedom flight-dynamics simulation. The transition is represented as a quasi-steady level acceleration from hover to wing-borne flight. At each speed V, the wing lift $L(V,\alpha)$ progressively reduces the thrust required from the lift rotors:

$$T_L(V) = \max\left[W - L(V,\alpha), 0\right]. \tag{28}$$

The cruise propulsors provide the thrust required to overcome drag and accelerate the aircraft,

$$T_C(V) = D(V,\alpha) + m_{TO}\dot{V}, \tag{29}$$

where $\dot{V}$ is the prescribed transition acceleration. The corresponding transition power is estimated as

$$P_{el,tr}(V) = \frac{\kappa_L T_L(V)^{3/2}}{\eta_{m,L}\sqrt{2\rho A_H}} + \frac{T_C(V)V}{\eta_{p,C}\eta_{m,C}}. \tag{30}$$

The transition energy is obtained by integration over the adopted speed schedule,

$$E_{tr} = \int_0^{V_{cr}} \frac{P_{el,tr}(V)}{\dot{V}}\, dV. \tag{31}$$

In the numerical performance indicators reported in Section 3.1, the range is interpreted as a preliminary wing-borne range estimate after vertical-flight and reserve-energy allocation. The transition term remains explicit in the general formulation because it is part of the aircraft-level energy balance, but it is not promoted to a separate numerical result unless a dedicated transition schedule and control law are available.

2.5 Mass consistency, trim and stability constraints

The sizing loop enforces the mass balance of Eq. (6). The reference case discussed in the paper is associated with the take-off mass reported in the preliminary sizing table of Section 3.1. The mass model is formulated as an aircraft-level mass-consistency problem rather than as a post-processing table or a bookkeeping exercise. For a candidate design, all mass items are evaluated from the same design state that defines the geometry, mission energy, hover sizing, cruise sizing and stability checks. The mass-balance residual is defined as

$$\varepsilon_m = \frac{m_{str} + m_{sys} + m_{prop,H} + m_{prop,C} + m_b + m_{pay} - m_{TO}}{m_{TO}}, \tag{32}$$

and the candidate is considered admissible only if $|\varepsilon_m|$ is lower than the adopted conceptual-design tolerance. If this condition is not met, the design is not interpreted as a mass-consistent aircraft and the sizing variables, propulsion selection or energy allocation must be revised.

The individual mass terms are linked to the physical drivers of the configuration. The structural mass is associated with the lifting-system geometry, the two-wing load sharing, the vertical tip-wings, the lateral booms carrying the lift rotors, the fuselage integration and the assumed load and material set. The hover-propulsion mass is obtained from the required hover thrust, power, torque, number of rotors and rotor diameter, using the adopted motor and propeller database or an equivalent regression. The cruise-propulsion mass is evaluated from the forward-flight thrust, shaft power, torque, rotational-speed and propeller-diameter requirements. The battery mass is obtained as the positive residual of the prescribed take-off mass after the structural, systems, propulsion and payload masses have been evaluated. The corresponding usable energy is then checked against the assumed battery specific energy, reserve policy and operational margins. Systems and payload masses are retained as explicit terms so that changes in mission requirement or equipment assumptions directly affect the aircraft mass balance. Table 3 reports the mass groups used to enforce aircraft-level mass consistency. Numerical entries are to be reported in the results section from the adopted structural assumptions, battery specification, motor database and payload definition.

The location of the centre of gravity is computed from the same mass groups used in the aircraft mass balance. In hover, the nominal centre of gravity is placed close to the centre of the thrust of

Table 3 – Mass groups used for the aircraft-level mass consistency of the reference configuration.

Mass group	Symbol	Evaluation in the sizing loop
Aircraft take-off mass	m_{TO}	Prescribed reference value reported in the sizing table
Airframe structure	m_{str}	Geometry- and load-dependent estimate for wings, vertical tip-wings, booms and fuselage integration
Systems and equipment	m_{sys}	Equipment, flight-control, wiring, landing and installation allowances
Hover propulsion	$m_{prop,H}$	Rotor, motor and installation mass from hover thrust, power, torque, N_H and D_H
Cruise propulsion	$m_{prop,C}$	Propeller and motor mass from cruise thrust, shaft power, torque, speed and diameter constraints
Battery system	m_b	Positive residual of prescribed m_{TO} after the other mass groups; usable energy checked through e_b, reserve policy and operational margins
Payload	m_{pay}	Mission requirement and payload definition
Total propulsion	m_{prop}	$m_{prop,H} + m_{prop,C}$

the vertical-lift rotor system to guarantee, in the nominal symmetric condition, an equal distribution of the thrust among the rotors devoted to hover, take-off and landing. This is a useful architectural criterion, but it does not by itself guarantee acceptable controllability. The method therefore requires a centre-of-gravity envelope and corresponding rotor-thrust margins to be checked as the payload and system layout are refined.

For wing-borne flight, longitudinal trim is imposed through the pitching-moment equilibrium and is written as

$$C_m(\alpha, \delta_e, x_{CG}) = 0, \tag{33}$$

where δ_e denotes the relevant longitudinal control variable or equivalent differential-control action. Static stability is imposed through a positive static margin,

$$SM = \frac{x_{NP} - x_{CG}}{\bar{c}_{ref}}, \qquad SM_{min} \leq SM \leq SM_{max}, \tag{34}$$

where x_{NP} is the neutral-point position and $\bar{c}_{ref}$ is a reference chord of the complete lifting system. The admissible interval for SM is not assigned as a universal constant. It must be selected consistently with the control authority, mission envelope and handling-quality requirements of the final vehicle.

2.6 Transition from full-scale concept to scaled prototyping

The scaled model is introduced after the conceptual design phase to verify the physical integration of the architecture and to support the preparation of subsequent experimental activity. Its role is primarily functional. It allows the arrangement of the box-wing system, lift rotors, cruise propulsors, lateral booms, door mechanism, internal installation and control hardware to be assessed on a physical platform. In the adopted implementation, the lift rotors are housed inside the lateral booms that connect the front and rear portions of the box-wing system, with a door mechanism intended to avoid detrimental aerodynamic effects during the cruise phase. The door mechanism is considered as a specific propulsion-airframe integration item: it must provide adequate clearance for rotor deployment and stowage, limit the aerodynamic exposure of inactive lift propulsors during cruise, avoid interference with the booms and rotor disks, and remain accessible for inspection and maintenance.

The upper doors are opened during vertical-lift operation to expose the rotor disks and are closed during the cruise or CTOL configuration to recover a cleaner external shape. When the lift rotors are switched off, a permanent-magnet indexing system is used to park the two-blade propellers in a longitudinal position, allowing the blades to be contained within the boom volume before door closure.

The scaled prototype is not used as a direct validation of the full-scale aerodynamic efficiency, range, hover power, acoustic footprint or certification-level safety. A reduced-scale aircraft cannot simultaneously preserve Reynolds number, Froude scaling, Mach number, structural flexibility, rotor disk

loading, motor dynamics and control bandwidth. For this reason, the interpretation of the scaled tests is limited to the maturity of the design concept and to the demonstration of selected architectural functions. Full-scale performance predictions remain those obtained from the conceptual design model and from subsequent aerodynamic, structural and flight-dynamic analyses.
This distinction is central to the present methodology. The scaled aircraft is a bridge between paper design and physical implementation, not a replacement for high-fidelity full-scale validation. Its value lies in exposing integration issues that are often hidden in purely numerical conceptual studies: available internal volume, accessibility of components, blade alignment and storage, interference between moving parts, cable routing, maintenance access and practical flight-control implementation.
The reference configuration used for this integration step is sketched in Fig. 2.

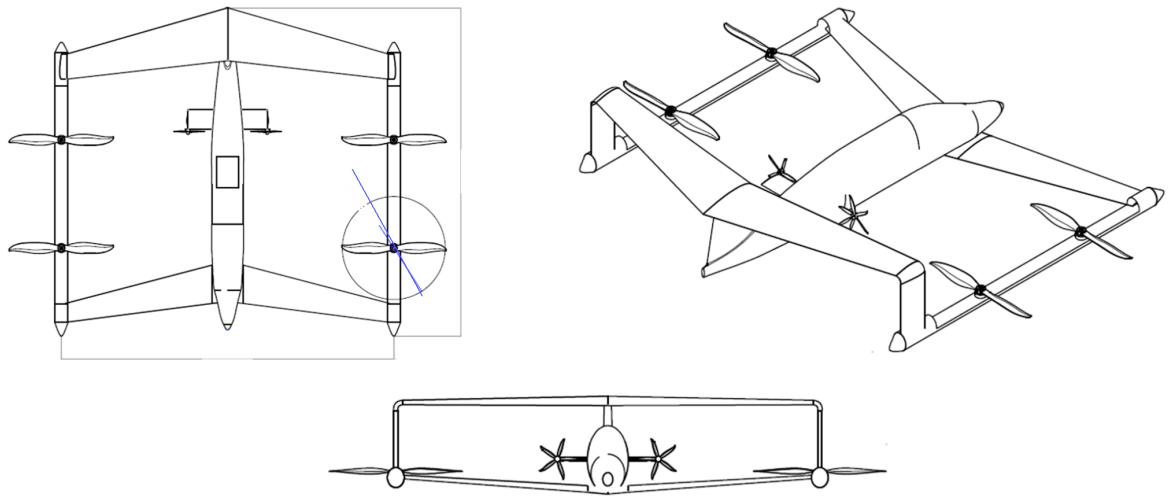


Figure 2 – Reference box-wing lift-and-cruise configuration used for the scaled prototype, shown through plan, perspective and front-view sketches.

2.7 Advancement over previous studies and current limitations

The methodological contribution of the paper is the combination of three elements: a box-wing lifting system, a lift-and-cruise propulsion architecture and a design-to-prototype development path for low-altitude civil missions. Previous conceptual studies on eVTOL aircraft and box-wing configurations provide the technical background for individual parts of the problem [11, 28]. The present workflow connects these elements in a single preliminary design process, with explicit attention to mass-energy estimation, propulsive separation, rotor integration in the closed lifting system and the functional role of the scaled demonstrator.
The present modelling scope is deliberately kept at conceptual-design fidelity. Aerodynamic analysis is limited to attached-flow and build-up estimates; separated flow, rotor slipstream interaction, propeller-wing interference, door-open aerodynamics and aeroacoustics require dedicated analyses. The transition model is quasi-steady and serves as a sizing-level energy and power check. Structural mass, motor and propeller selection, stability constraints and trim capability are treated consistently with this level of fidelity, while flight-dynamic handling qualities, control allocation, gust response and failure cases remain part of the subsequent modelling and test programme. The scaled prototype supports the development of the architecture by documenting physical integration, manufacturability and functional operation of the stowage concept within the selected scale.

3. Reference configuration, scaled prototype and preliminary verification

3.1 Baseline and refined design preliminary performance assessment

The design-to-performance chain described in Section 2. is here applied to two numerical states of the same box-wing lift-and-cruise architecture. The first state is denoted as the baseline design. It corresponds to the reference configuration and to the geometry used to guide the scaled prototype

integration. The second state is denoted as the refined design. It is obtained by applying the same sizing method with an endurance/range-driven ranking criterion, while preserving the same architectural class, namely a box-wing lifting system, four vertical-lift rotors housed in lateral booms and two dedicated cruise propulsors.

This distinction is introduced only at the results level. The baseline and refined designs are not two unrelated aircraft. They are two feasible design states generated within the same conceptual search domain. Their comparison is useful because it shows how the architecture responds when the sizing loop modifies the main geometric, energetic and propulsive variables under the feasibility constraints reported in Table 2. The comparison is not intended to prove a global optimum, but to quantify the effect of the refined sizing state on disk loading, installed energy, wing loading, cruise power, endurance and wing-borne range.

The reported indicators are divided into design-state quantities and derived quantities. The design-state quantities include take-off mass, payload, battery mass, installed energy, wing span, reference area, rotor diameter and propeller diameter. The derived quantities include wing loading, disk loading, hover energy allocation, cruise endurance, wing-borne range and cruise energy consumption. This distinction remains relevant because every derived indicator depends directly on the adopted design-state quantities and on their reported precision.

Table 4 – Baseline and refined design states obtained from the preliminary sizing workflow.

Quantity	Baseline design	Refined design	Design note
Aircraft class	Four passengers plus one pilot	Four-passenger class payload	Civil low-altitude eVTOL platform
Take-off mass, m_{TO}	2200 kg	2900 kg	Adopted sizing values
Payload	475 kg	475 kg	Passenger-class payload assumption
Airframe, systems and propulsion-installation mass	1210 kg	1593.3 kg	Aggregated values at available precision
Battery mass	515 kg	829 kg	Residual mass from the aircraft mass balance
Installed battery energy	103.0 kWh	165.8 kWh	Based on 200 Wh/kg battery specific energy
Wing span, b	12.50 m	14.00 m	Compact box-wing span
Total wing reference area, S	33.4 m^2	45.9 m^2	$S = S_1 + S_2$
Wing loading, m_{TO}/S	65.9 kg/m^2	63.2 kg/m^2	Derived sizing indicator
Lift rotors, N_H	4 two-blade rotors	4 two-blade rotors	Dedicated vertical-lift system
Lift-rotor diameter, D_H	3.94 m	5.08 m	Large low-disk-loading rotors
Total lift-disk area, A_H	48.7 m^2	81.1 m^2	$A_H = N_H \pi D_H^2/4$
Disk loading, m_{TO}/A_H	45.2 kg/m^2	35.8 kg/m^2	Derived from take-off mass and lift-disk area
Cruise propulsors	2 fixed propulsors	2 fixed propulsors	Dedicated wing-borne thrust system
Cruise propeller diameter	2.10 m	1.84 m	Preliminary propeller sizing
Cruise speed	151.0 km/h	147.7 km/h	Sizing cruise condition
Hover power, total	558.2 kW	588.0 kW	Power associated with the prescribed 5 min hover allocation
Cruise propulsion power, total	145.3 kW	90.9 kW	Preliminary installed-power sizing entry
Hover energy allocation	46.5 kWh	49.0 kWh	Derived from the prescribed hover time
Estimated cruise L/D	17.2	17.1	Build-up/VLM-level estimate for attached cruise condition
Cruise endurance	19.1 min	63.1 min	Wing-borne endurance after hover and reserve-energy allocation
Estimated wing-borne range	48.0 km	155.4 km	After prescribed hover and reserve allocations
Cruise energy consumption	962 Wh/km	615 Wh/km	Derived from cruise energy and range
Clean $C_{L,\max}$ used for stall check	1.20	1.20	Conservative preliminary 14%-thick-airfoil/plain-flap assumption; no complex high-lift system

Table 4 should be read as a quantitative trace of the sizing workflow. For a fixed aircraft class, the mass and battery entries determine the available energy. Wing span and reference area define the

wing loading and the cruise lift coefficient at the sizing speed. The aerodynamic build-up and VLM-induced contribution provide the cruise polar and the estimated lift-to-drag ratio. The rotor diameter fixes the total lift-disk area and hence the disk loading that drives the hover-power estimate. The remaining wing-borne energy, after the prescribed hover and reserve allocations, is then converted into cruise endurance and range through the cruise power calculated at the same design state.
The refined design modifies the energy and disk-loading balance in a quantitatively relevant way. Battery mass increases from 515.0 kg to 829 kg, corresponding to an installed-energy increase from 103.0 kWh to 165.8 kWh. The lift-rotor diameter increases from 3.94 m to 5.08 m; because disk area scales with the square of diameter, the total lift-disk area increases from 48.7 m^2 to 81.1 m^2. Consequently, although the refined design has a higher take-off mass, the disk loading decreases from 45.2 kg/m^2 to 35.8 kg/m^2. This reduction is directly relevant to the vertical-flight power balance and explains why the hover power remains of the same order, 558.2 kW for the baseline and 588.0 kW for the refined design, despite the larger aircraft mass. However, in the second case a higher torque is required.
The wing-borne part of the mission shows a more pronounced change. The refined design increases the wing span from 12.50 m to 14.00 m and the reference area to 45.9 m^2, while keeping the wing loading close to the baseline value, 63.2 kg/m^2 against 65.9 kg/m^2. At the same time, the estimated cruise propulsion power decreases from 145.3 kW to 90.9 kW. Within the preliminary model, this translates into a cruise endurance increase from 19.1 min to 63.1 min and an estimated wing-borne range increase from 48.0 km to 155.4 km. The associated cruise energy consumption decreases from 962 Wh/km to 615 Wh/km. These values should be interpreted as conceptual-design indicators, but they show that the refined design does not improve range only by adding battery energy. The improvement is produced by the coupled change in installed energy, disk loading, wing sizing, cruise power and propulsive operating point.
The electric-machine data are used at sizing level. Hover and cruise powers are reported because they are directly obtained from the propeller and mission-energy calculations. The final torque-speed matching of the cruise motor, the inverter limits, the thermal derating policy and the possible transmission architecture are not used here to claim definitive propulsion-installation maturity. This separation avoids mixing a conceptual performance estimate with a detailed motor-drive qualification that belongs to a later design phase.
The baseline-refined comparison also clarifies the architectural relevance of the rotor-stowage solution. The lift rotors are deliberately large in order to keep disk loading low during vertical operation. The refined design reinforces this trend, increasing the rotor diameter while further reducing disk loading. The same choice would normally increase the aerodynamic penalty of a lift-and-cruise aircraft in forward flight if the inactive rotors remained exposed. Their integration inside the lateral booms is therefore part of the mission-level efficiency rationale of the configuration, because it connects hover efficiency, packaging and cruise aerodynamic cleanliness within the same design logic.

3.2 Scaled prototype development

The reference configuration was translated into a dynamically reduced scaled model to assess the feasibility of the selected integration choices. The model scale is 1:8, with an overall length of approximately 1.55 m and a span of approximately 1.60 m. These dimensions make the demonstrator suitable for handling, bench checks and initial ground operation while preserving the recognizable layout of the full-scale concept. The model is not interpreted as a full dynamic-similarity replica. Its function is to preserve the architectural arrangement, the distribution of the main components, the interaction between the box-wing and the lift-and-cruise propulsion system, and the mechanical accessibility of the selected solution.
The two principal configuration states are shown in Fig. 3. In the cruise or CTOL arrangement, the lift rotors are contained inside the lateral booms and the upper doors are closed, reducing their external exposure. In the VTOL arrangement, the doors are open and the vertical-lift propulsors are exposed for rotor-borne operation. The booms therefore act as structural connectors, aerodynamic fairings and propulsion-integration volumes. Their role is central to the proposed architecture because they mitigate a recurring weakness of lift-and-cruise vehicles: the presence of lift propulsors that are necessary for vertical flight but inactive during cruise.



(a) Closed-boom arrangement representative of cruise or CTOL operation.



(b) Open-boom arrangement with the vertical-lift propulsors exposed.

Figure 3 – Scaled demonstrator in the two main configuration states used to verify the integration of the box-wing lifting system with the lift-and-cruise propulsion layout.

The doorway mechanism and the blade-parking concept are detailed in Fig. 4. The permanent-magnet indexing system is used to align the two-blade propellers with the boom axis after motor shutdown. This avoids an arbitrary blade stop position before door closure and reduces the risk of local interference between blades, doors and the internal boom volume. For this demonstrator, the relevant prototype-level evidence concerns the physical compatibility of the stowage sequence and of the opening and closing arrangement. Quantitative aerodynamic benefits in cruise will be assessed through dedicated aerodynamic analysis and subsequent experimental activity.



Figure 4 – Detail of an opened lateral boom showing the lift-propeller installation, the longitudinal blade-parking condition and the door aperture used for VTOL operation.

3.3 Manufacturing and system integration

The prototype documentation indicates a modular manufacturing approach, in which the fuselage, wings, vertical tip-wings, lateral booms and propulsion modules are prepared as separate assemblies and then aligned into the closed lifting system. Figure 5 illustrates two representative stages of this process. The manufacturing route is relevant to the design argument because the proposed architecture requires more than the placement of rotors around a conventional airframe. The booms must accommodate the lift motors and propellers, provide sufficient stiffness and alignment between front and rear lifting elements, allow the door mechanism to operate without interference, and preserve access for inspection and maintenance.

The large fuselage access panel is especially relevant because battery packs, electronic speed controllers, wiring, flight-control hardware and the autopilot must remain accessible without compromis-

ing the closed-wing layout. The integration sequence therefore remains part of the architectural assessment, since the closed lifting system, the lateral booms and the propulsion installation must be compatible with assembly, inspection and preparation of the demonstrator.



(a) Intermediate assembly state used to align fuselage, wings and lateral booms.



(b) Bench integration state showing fuselage access and cruise-propulsion installation.

Figure 5 – Manufacturing and integration stages of the scaled demonstrator, with emphasis on modular assembly, accessibility and propulsion-airframe integration.

3.4 Ground verification and initial taxi activity

After assembly, the model was used for prototype-level checks before the extension toward a dedicated flight-test campaign. The activity included bench verification, static propulsion checks, functional checks of door opening and closure, verification of blade parking and stowage, inspection of accessible installations, ground handling and initial low-speed taxi runs. These checks provide evidence that the architecture can be assembled, inspected, actuated and operated at low speed without changing the basic design logic.

The ground-test configuration is shown in Fig. 6. The image is used to document the readiness level of the demonstrator and the coherence between the conceptual arrangement and the physical aircraft. The observations obtained at this stage concern configuration integrity, ground handling, accessibility and operational preparation. The continuation of the experimental programme will extend this evidence toward transition performance, closed-loop flight-dynamic behaviour, hover and cruise efficiency, and acoustic response through dedicated instrumentation, flight-test procedures and higher-fidelity analysis.



Figure 6 – Scaled demonstrator positioned on the outdoor test area during preliminary ground-handling and low-speed taxi activity.

3.5 Discussion of the prototype-level evidence

The main information obtained from the prototype is architectural. The model shows that the combination of a box-wing lifting system and a lift-and-cruise propulsion layout can be translated into a physically consistent arrangement in which the inactive lift rotors are not left as exposed appendages during cruise. This point is important because the lift-and-cruise concept is often attractive at the functional level, but it tends to transfer part of the design difficulty to the integration of the unused lift system in wing-borne flight. In the proposed configuration, this difficulty is addressed by the lateral booms, which perform several functions at the same time: they connect the front and rear lifting elements, house the vertical-lift propulsors, provide the volume required for blade stowage, support the door mechanism and contribute to the external cleanliness of the cruise configuration.

The scaled demonstrator also clarifies practical aspects that are difficult to assess from conceptual drawings alone. These include the clearance between blades and doors, the repeatability of blade parking before closure, the available space for wiring and propulsion components, the accessibility of batteries and avionics, and the assembly sequence of the closed lifting system. These observations complement the subsequent aerodynamic and flight-dynamic validation activity by reducing the risk of pursuing a configuration that is attractive on paper and impractical in hardware. The prototype therefore provides design-to-prototype evidence that supports the next quantitative assessment steps.

The current level of maturity suggests a clear continuation of the work. The next experimental phase should extend the present ground-test and integration activity toward a dedicated flight-test campaign, including transition manoeuvres, closed-loop control tuning and quantitative flight-dynamic assessment. In parallel, the conceptual performance estimates should be consolidated through detailed aerodynamic interference modelling of the open and closed boom states, refined propulsion maps, structural sizing of the closed-wing load path, aeroacoustic assessment and a complete control-allocation model for nominal and degraded configurations.

4. Conclusions

This paper presented the design rationale, conceptual sizing methodology and scaled prototype implementation of a civil box-wing lift-and-cruise eVTOL configuration for low-altitude economy applications. The study was motivated by the need for aircraft architectures that are not optimized only for vertical take-off, but for the complete mission, including hover, transition, cruise, ground operation, maintainability and integration with limited infrastructure. Within this framework, the box-wing lifting system was considered as a compact closed architecture suitable for hosting a separated lift-and-cruise propulsion layout.

The baseline and refined designs were reported through a consistent set of mass, geometry, propulsion and energy indicators. Their comparison documents the transition from design variables to performance estimates after the methodology has been defined. Take-off mass, battery allocation, wing geometry and rotor diameter define the energy and aerodynamic problem; hover power, cruise power, endurance and range are then obtained as derived quantities of the same sizing state. The refined design shows, at conceptual level, that range improvement is produced by the coupled change of installed energy, disk loading, wing sizing and cruise power rather than by battery increase alone. The baseline aircraft is a four-passenger plus one-pilot class configuration with a take-off mass of 2200 kg, a 12.50 m span, a total wing reference area of 33.4 m^2 and four large lift rotors housed in lateral booms.

The principal architectural contribution is the integration of the inactive lift rotors inside faired lateral booms during cruise. These booms are not treated as simple structural supports. They connect the box-wing elements, contain the vertical-lift propulsors, support door opening and closure, enable blade stowage through a longitudinal parking condition and reduce the exposed inactive-rotor installation in wing-borne flight. This addresses one of the main penalties of lift-and-cruise aircraft while avoiding the mechanical complexity of tilting large lifting surfaces or propulsors.

The scaled model was presented as a functional demonstrator of the design-to-prototype process. Its role is not to validate full-scale performance directly, but to verify the physical compatibility of the architecture, the manufacturability of the closed lifting system, the accessibility of the internal instal-

lations, the integration of propulsion and control hardware, the operation of the door and stowage mechanism, and the preparation for further experimental activity. Preliminary bench checks, functional ground checks and initial low-speed taxi activity provide integration-level evidence that the layout can be built and operated at prototype level.

Subsequent work will extend the present ground-test and integration activity toward a dedicated flight-test campaign, including transition manoeuvres, closed-loop control tuning and quantitative flight-dynamic assessment. Further developments will also include higher-fidelity aerodynamic interference analysis of the open and closed boom configurations, refined motor-propeller matching, battery-pack consolidation, structural sizing of the box-wing and boom load paths, aeroacoustic assessment and a consolidated mission-level performance evaluation.

5. Contact Author Email Address

The corresponding author is Karim Abu Salem, mail to: karim.abusalem@unitn.it

6. Copyright Statement

The authors confirm that they, and/or their company or organization, hold copyright on all of the original material included in this paper. The authors also confirm that they have obtained permission, from the copyright holder of any third party material included in this paper, to publish it as part of their paper. The authors confirm that they give permission, or have obtained permission from the copyright holder of this paper, for the publication and distribution of this paper as part of the ICAS proceedings or as individual off-prints from the proceedings.

References

[1] H. Huang, J. Su, and F.-Y. Wang. The potential of low-altitude airspace: The future of urban air transportation. *IEEE Transactions on Intelligent Vehicles*, 9, 2024. doi: 10.1109/TIV.2024.3483889.

[2] A. Bauranov and J. Rakas. Designing airspace for urban air mobility: A review of concepts and approaches. *Progress in Aerospace Sciences*, 125:100726, 2021. doi: 10.1016/j.paerosci.2021.100726.

[3] A. P. Cohen, S. A. Shaheen, and E. M. Farrar. Urban air mobility: History, ecosystem, market potential, and challenges. *IEEE Transactions on Intelligent Transportation Systems*, 22, 2021. doi: 10.1109/TITS.2021.3082767.

[4] Y. Zhou. Unmanned aerial vehicles based low-altitude economy with lifecycle techno-economic-environmental analysis for sustainable and smart cities. *Journal of Cleaner Production*, 499:145050, 2025. doi: 10.1016/j.jclepro.2025.145050.

[5] Z. Meng et al. eVTOL aircraft for the low-altitude economy: A review of development history, core technologies, and future trends. *Case Studies on Transport Policy*, 22:101629, 2025. doi: 10.1016/j.cstp.2025.101629.

[6] G. A. Misté, G. Venturelli, and E. Benini. Mobility impact assessment of innovative aircraft inside the european multimodal transport network. In *AIAA AVIATION 2021 Forum*, pages AIAA Paper 2021–2952, 2021. doi: 10.2514/6.2021-2952.

[7] A. M. Johnson, C. J. Cunningham, E. Arnold, W. D. Rosamond, and J. K. Zègre-Hemsey. Impact of using drones in emergency medicine: What does the future hold? *Open Access Emergency Medicine*, 13:487–498, 2021. doi: 10.2147/OAEM.S247020.

[8] V. Engesser, E. Rombaut, L. Vanhaverbeke, and P. Lebeau. Autonomous delivery solutions for last-mile logistics operations: A literature review and research agenda. *Sustainability*, 15(3):2774, 2023. doi: 10.3390/su15032774.

[9] S. Jordan, J. Moore, S. Hovet, J. Box, J. Perry, K. Kirsche, D. Lewis, and Z. T. H. Tse. State-of-the-art technologies for UAV inspections. *IET Radar, Sonar & Navigation*, 12(2):151–164, 2018. doi: 10.1049/iet-rsn.2017.0251.

[10] K. Ranasinghe, R. Sabatini, A. Gardi, S. Bijjahalli, R. Kapoor, T. Fahey, and K. Thangavel. Advances in integrated system health management for mission-essential and safety-critical aerospace applications. *Progress in Aerospace Sciences*, 128:100758, 2022. doi: 10.1016/j.paerosci.2021.100758.

[11] G. Palaia, K. Abu Salem, V. Cipolla, V. Binante, and D. Zanetti. A conceptual design methodology for e-VTOL aircraft for urban air mobility. *Applied Sciences*, 11(22):10815, 2021. doi: 10.3390/app112210815.

[12] A. Bacchini and E. Cestino. Electric VTOL configurations comparison. *Aerospace*, 6(3):26, 2019. doi: 10.3390/aerospace6030026.

[13] N. Pongsakornsathien, N. E.-D. Safwat, Y. Xie, A. Gardi, and R. Sabatini. Advances in low-altitude airspace management for uncrewed aircraft and advanced air mobility. *Progress in Aerospace Sciences*, 154:101085, 2025. doi: 10.1016/j.paerosci.2025.101085.

[14] A. Bacchini, E. Cestino, B. Van Magill, and D. Verstraete. Impact of lift propeller drag on the performance of eVTOL lift+cruise aircraft. *Aerospace Science and Technology*, 109:106429, 2021. doi: 10.1016/j.ast.2020.106429.

[15] T. Pattanayak and D. Mavris. Battery technology for sustainable aviation: A review of current trends and future prospects. *Applied Energy*, 397:126356, 2025. doi: 10.1016/j.apenergy.2025.126356.

[16] K. Abu Salem, G. Palaia, and A. A. Quarta. Review of hybrid-electric aircraft technologies and designs: Critical analysis and novel solutions. *Progress in Aerospace Sciences*, 141:100924, 2023. doi: 10.1016/j.paerosci.2023.100924.

[17] J. Xu, C. Guan, Y. Wang, J. Zhuang, and W. Gan. A systematic review of urban air mobility development: eVTOL drones' technological challenges and low-altitude policies of shenzhen. *Drones*, 9(12):842, 2025. doi: 10.3390/drones9120842.

[18] G. Palaia, K. Abu Salem, and A. A. Quarta. Parametric analysis for hybrid–electric regional aircraft conceptual design and development. *Applied Sciences*, 13(19):11113, 2023. doi: 10.3390/app131911113.

[19] A. Elmeligy, N. E.-D. Safwat, M. S. El-Moursi, and R. Sabatini. Energy production, storage and management for sustainable VTOL aircraft and advanced air mobility. *Energy Reports*, 15:109137, 2026. doi: 10.1016/j.egyr.2026.109137.

[20] N. E.-D. Safwat, A. Elmeligy, A. A. Almurshidi, and R. Sabatini. Hybrid-electric propulsion system for VTOL drones and sustainable air mobility. *IEEE Transactions on Aerospace and Electronic Systems*, 2026. Accepted/in press. doi: 10.1109/TAES.2026.3684457.

[21] S. Wang, L. T. L. Pereira, and D. Ragni. Design exploration of UAM vehicles. *Aerospace Science and Technology*, 160:110058, 2025. doi: 10.1016/j.ast.2025.110058.

[22] S. P. C. van Schie, M. L. Ruh, A. H. Fletcher, M. A. P. Warner, M. Z. Sperry, L. Scotzniovsky, N. C. Orndorff, R. Xiang, J. Yan, H. Zhao, J. J. Krokowski, J.-S. Chen, D. Sarojini, H. Gill, S. Lee, A. C. Tagg, R. Anderson, E. Green, C. Joseph, A. Ning, Z. Cheng, Z. Cao, C. Mi, A. T. Guibert, A. Cronk, H. A. Kim, Y. S. Meng, C. Silva, and J. T. Hwang. Large-scale distributed multidisciplinary design optimization of the NASA lift-plus-cruise air taxi concept. In *AIAA SCITECH 2025 Forum*, pages AIAA Paper 2025–0362, 2025. doi: 10.2514/6.2025-0362.

[23] M. L. Ruh, M. A. P. Warner, L. Scotzniovsky, A. H. Fletcher, M. Z. Sperry, and J. T. Hwang. System-level, large-scale multidisciplinary design optimization of an air taxi concept. *Journal of Aircraft*, pages 1–24, 2026. Articles in Advance. doi: 10.2514/1.C038533.

[24] M. L. Ruh, A. H. Fletcher, D. Sarojini, M. Z. Sperry, J. Yan, L. Scotzniovsky, S. P. C. van Schie, M. A. P. Warner, N. C. Orndorff, R. Xiang, A. J. Joshy, H. Zhao, J. Krokowski, H. Gill, S. Lee, Z. Cheng, Z. Cao, C. Mi, C. Silva, L. Wolfe, J.-S. Chen, and J. T. Hwang. Large-scale multidisciplinary design optimization of a NASA air taxi concept using a comprehensive physics-based system model. In *AIAA SCITECH 2024 Forum*, pages AIAA Paper 2024–0771, 2024. doi: 10.2514/6.2024-0771.

[25] O. Ugwueze, T. Statheros, N. Horri, M. A. Bromfield, and J. Simo. An efficient and robust sizing method for eVTOL aircraft configurations in conceptual design. *Aerospace*, 10(3):311, 2023. doi: 10.3390/aerospace10030311.

[26] K. Abu Salem, G. Palaia, and E. Carrera. A discussion on benchmarking unconventional configurations with conventional aircraft: The box-wing study case. *CEAS Aeronautical Journal*, 15:1069–1090, 2024. doi: 10.1007/s13272-024-00758-2.

[27] L. Prandtl. Induced drag of multiplanes. NACA Technical Note 182, National Advisory Committee for Aeronautics, 1924.

[28] K. Abu Salem, G. Palaia, A. Frediani, and E. Carrera. The box-wing configuration: A critical review of design approaches and applications. *Progress in Aerospace Sciences*, 157:101108, 2025. doi: 10.1016/j.paerosci.2025.101108.

[29] K. Abu Salem, G. Palaia, M. Carini, et al. A CFD-based collaborative approach for box-wing aircraft aerodynamic assessment: The PARSIFAL study case. *Aerotecnica Missili & Spazio*, 102:385–407, 2023. doi: 10.1007/s42496-023-00172-7.

[30] G. Palaia, K. Abu Salem, V. Cipolla, E. Di Vitantonio, E. Rizzo, and V. Binante. Preliminary design of a tiltwing UAV with a box wing configuration. *Aerotecnica Missili & Spazio*, 97(4):198–207, 2018. doi: 10.1007/BF03406054.

[31] V. Cipolla, A. Frediani, E. Lonigro, and F. Oliviero. Aerodynamic design of a light amphibious PrandtlPlane: Wind tunnel tests and CFD validation. *Aerotecnica Missili & Spazio*, 94:113–123, 2015. doi: 10.1007/BF03404694.

[32] C. Varriale, T. Lombaerts, and G. Looye. Direct lift control: A review of its principles, merits, current and future implementations. *Progress in Aerospace Sciences*, 152:101073, 2025. doi: 10.1016/j.paerosci.2024.101073.

[33] C. Zhao, Y. Yang, Z. Cheng, T. Zhang, and Y. Liu. Recent advancements and challenges for eVTOL aircraft aerodynamic noise in urban air mobility. *Progress in Aerospace Sciences*, 161:101184, 2026. doi: 10.1016/j.paerosci.2026.101184.

[34] E. L. Thompson, A. G. Taye, W. Guo, P. Wei, M. Quinones-Grueiro, I. Ahmed, G. Biswas, J. Quattrociocchi, S. Carr, U. Topcu, J. Jones, and M. Brittain. A survey of eVTOL aircraft and AAM operation hazards. In *AIAA AVIATION 2022 Forum*, pages AIAA Paper 2022–3539, 2022. doi: 10.2514/6.2022-3539.

[35] J. He, Q. He, Z. Xu, Y. Jia, J. Wang, K. Li, and W. Tan. Key technologies and upgrade strategies for eVTOL aircraft energy storage systems. *Journal of Energy Storage*, 103:114402, 2024. Part B. doi: 10.1016/j.est.2024.114402.

[36] J. Zhang, Y. Liu, and Y. Zheng. Overall eVTOL aircraft design for urban air mobility. *Green Energy and Intelligent Transportation*, 3(2):100150, 2024. doi: 10.1016/j.geits.2024.100150.

[37] Daniel P. Raymer. *Aircraft Design: A Conceptual Approach*. AIAA Education Series. American Institute of Aeronautics and Astronautics, Washington, DC, 1992. ISBN 0-930403-51-7.

[38] Mark Drela and Harold Youngren. *AVL 3.36 User Primer*, 2017. Online software manual. Available online: `https://perma.cc/R35R-W29F`.

[39] A. Frediani and G. Montanari. Best wing system: An exact solution of the prandtl's problem. In *Variational Analysis and Aerospace Engineering*, volume 33 of *Springer Optimization and Its Applications*, pages 183–211. Springer, New York, NY, 2009. doi: 10.1007/978-0-387-95857-6_11.

[40] L. Demasi, A. Dipace, G. Monegato, and R. Cavallaro. Invariant formulation for the minimum induced drag conditions of nonplanar wing systems. *AIAA Journal*, 52(10):2223–2240, 2014. doi: 10.2514/1.J052837.

[41] A. Savino and A. Zanotti. Aerodynamic interaction between wing and propeller in eVTOL airplane mode flight condition. *CEAS Aeronautical Journal*, 2025. doi: 10.1007/s13272-025-00871-w.

[42] R. de Vries, A. K. Jeyaraj, F. Salucci, A. Brown, M. A. Clarke, P. J. Ansell, M. F. M. Hoogreef, B. Zaghari, S. Liscouët-Hanke, R. Love, M. Ilak, and G. Cinar. Conceptual design of electrified aircraft: A practical guide for engineering students and practitioners. In *AIAA AVIATION 2026 Forum*, pages AIAA Paper 2026–4690, 2026. doi: 10.2514/6.2026-4690.

[43] Barnes W. McCormick. *Aerodynamics of V/STOL Flight*. Dover Publications, 1999.

[44] EMRAX d.o.o. EMRAX 268 electric motor specifications, 2026. Manufacturer technical page. Available online: `https://emrax.com/e-motors/emrax-268/`. Accessed 7 July 2026.

[45] EMRAX d.o.o. EMRAX 348 electric motor specifications, 2026. Manufacturer technical page. Available online: `https://emrax.com/e-motors/emrax-348/`. Accessed 7 July 2026.

[46] Siemens AG. Record-setting electric aircraft motor SP260D factsheet, 2016. Technical factsheet for the SP260D and Extra 330LE. Available online: `https://assets.new.siemens.com/siemens/assets/api/uuid:04c7fe39-b322-417f-a3ac-7bcae1d64d50/factsheet-erstflug-weltrekordmotor-d.pdf`. Accessed 7 July 2026.